Surface structure of Ge(100) studied by He diffraction

W. R. Lambert, P. L. Trevor, M. J. Cardillo, A. Sakai,* and D. R. Hamann

AT&T Bell Laboratories, Murray Hill, New Jersey 07974

(Received 6 November 1986)

The surface structure of Ge(100) has been studied by use of the technique of He diffraction. At room temperature the surface shows an apparent sharp (2×1) periodicity with additional contributions extending through the quarter-order beam positions of the $c(4 \times 2)$. For surface temperatures $T \leq 150$ K, the surface nearly completely orders into a $c(4 \times 2)$ with a residual contribution from an apparent (2×2) component. We compare the experimental results to eikonal scattering calculations based on surface potentials generated using a modified charge-superposition scheme. We find that the alternating tilted dimer model is most consistent with the experimental diffraction spectra, specifically for a dimer tilt angle of $6° \pm 2°$. The sensitivity of He diffraction to the Ge(100) surface structure is discussed.

I. INTRODUCTION

We have studied the Ge(100) surface structure using the technique of He diffraction. We find that at $T \leq 150$ K the surface periodicity is nearly ordered into $c(4 \times 2)$. At room temperature the surface structure appears to be a sharp (2×1) but with additional intensity streaks extending through the quarter-order positions of the $c(4 \times 2)$. The disordering of the $c(4 \times 2)$ appears continuous over the studied temperature range. The diffraction angular scans contain rainbow and supernumerary rainbow maxima characteristic of a strongly corrugated He-surface potential. We utilize the modified atomic charge superposition (MACS) scheme[1] to generate scattering potentials for model structures to compare with the data. We find the alternating tilted dimer model [a $c(4 \times 2)$ structure] fits the data well, specifically with a dimer bond tilt angle of $6° \pm 2°$. We examine the sensitivity of the fit to model parameters, discuss the implications of the surface disorder, and the structural correspondence of the Ge(100) and Si(100) surfaces.

The structural similarity of Ge(100) and Si(100) has been recognized for some time. For Si(100) the original proposed dimerization[2] and subsequently proposed tilting[3] of the dimer bond has been theoretically shown to be energetically favored. The long-range ordering of the tilted dimers is beyond present theoretical accuracy but different periodic arrangements are expected to be nearly degenerate in energy[3] implying that steps and defects may play an important role in surface order.[4] Experimental evidence including low-energy electron diffraction (LEED),[5-10] He diffraction,[11] ion scattering,[12] and high-resolution photoemission[13] strongly suggests that the underlying structural unit of both surfaces is the same. In particular, He diffraction results clearly indicate that the apparent (2×1) surfaces observed at room temperature are similarly disordered and for Ge(100) can be continuously correlated to the nearly ordered $c(4 \times 2)$ periodicity as observed at low temperatures using several techniques.[9,12-14] Recently, the room temperature reconstructed Si(100) surface has been studied using scanning tunneling microscopy.[15] A surface consisting of a mixed configuration of buckled and unbuckled dimer periodicities, the specific structure of which appear to be related to surface defect and step densities, was observed. This result confirms the conclusions about the surface structure based on analysis of He-diffraction experiments.[1]

II. EXPERIMENT

The experimental apparatus is a modification of a previously described system.[16] The essential features are a UHV scattering chamber which includes an Auger spectrometer (AES), LEED, Ar^+ sputtering source, and a rotatable, differentially pumped mass spectrometer used to detect the in-plane scattered He beam at a distance of 12 cm from the crystal. The base pressure of the chamber is $\sim 2 \times 10^{-10}$ Torr. The crystal was mounted on a sapphire plate attached to Cu blocks. The crystal could be cooled to ~ 130 K (using liquid nitrogen) as calibrated from independent experiments, and heated as high as necessary using electron bombardment from a tungsten filament. The crystal assembly could be rotated about both the polar angle, θ, and azimuthal angle, ϕ.

The He beam source could be cooled to ~ 100 K. For a nozzle diameter of 25 μm and a He pressure of ~ 30 atm, the incident He velocity (wavelength) distributions have a normalized full width half maximum (FWHM) of 0.8% at 100 K ($\lambda \sim 1$ Å) and ~ 2.0% at 300 K (0.57 Å). The incident He beam was square-wave modulated, typically at 100 Hz, and collimated to 0.2° so as to illuminate a 1×2 mm^2 rectangular area at the crystal surface which was located 35 cm from the nozzle. The effective He diffraction angular resolution is $\sim 1°$ and is determined by the 2 mm lateral spread of the incident He beam at the crystal surface. From computer-simulated He trajectories, a resolution, defined by a 90% falloff of a diffraction-peak intensity, was calculated to correspond to a symmetrical area of reciprocal space (along both the [01] and [11] lattice directions) of 8% of the spacing between integer diffraction peaks. The shape of the analyzer resolution is relatively independent of the scattering angle. The

observed linewidths of all the sharp diffraction features are determined by the detector resolution. The reciprocal space resolution determines the extent to which we are able to resolve the two-dimensional ordering information inherent in the temperature dependence of the streak intensity. The He diffraction resolution corresponds approximately to coherence distances on the surface of the order of 10^2 Å.

The Ge(100) crystals were cut to within 0.5° of the [001] plane and had an active nominal impurity level of 10^{14} cm^{-3} and a resistivity of 30 Ω cm. Following several days of cyclic Ar$^+$ sputtering and annealing at ~ 900 K to remove surface oxides and polishing damage, a clean surface was obtained as determined by AES, with carbon being the only detectable impurity (typical [C]/[Ge] AES ratio ~ 0.015). A sharp two-domain (2×1) pattern with a qualitatively low background could be visually observed with LEED at room temperature. Over a period of several weeks of experimentation and repeated sputtering and annealing cycles, the extra intensity streaks persistently seen with He diffraction became visible at room temperature on the display LEED device (see Fig. 1).

The alignment of the crystal normal with respect to the plane defined by the rotation of the mass-spectrometer detector is critical for obtaining accurate diffraction intensities, particularly for narrow-wavelength distributions.
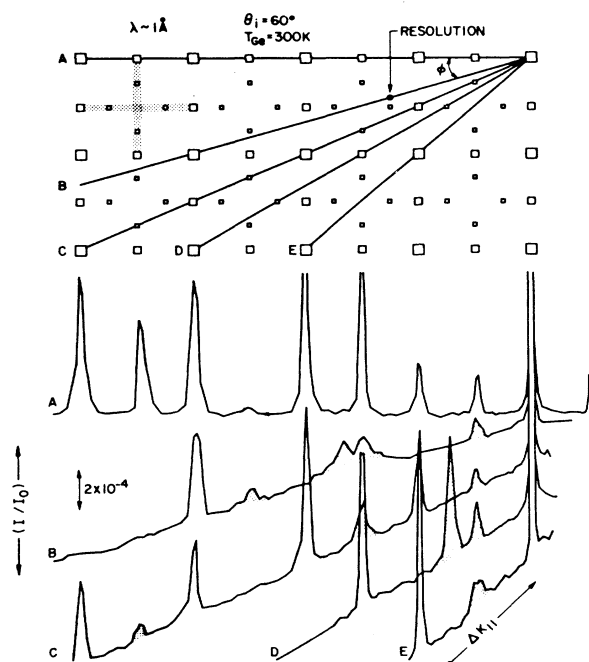

FIG. 1. He diffraction scans of Ge(100) at 300 K for different azimuthal angles, $\phi =$ (a) 0.0°, (b) 18.4°, (c) 26.6°, (d) 33.7°, and (e) 45.0° for an incident scattering angle of $\theta_i = 60$° and an incident He wavelength of $\lambda = 1$ Å. The reduced intensities are plotted against $\Delta K_{\parallel}$ the reciprocal lattice coordinate, and the abscissa is rotated by the azimuthal angle ϕ, providing a direct vertical correspondence between the reciprocal nets as observed in LEED and atom diffraction. The features associated with the disordered $c(4 \times 2)$ and $c(2 \times 2)$ periodicities are shaded for emphasis.

In-plane and azimuthal alignment was accomplished by iterative intensity maximization of the specular beam at different incident angles and for diffraction beams far from specular. The diffraction alignment was routinely checked and optimized as the temperature was changed.

III. RESULTS

A. Periodicity

The equilibrium surface periodicity of Ge(100) remains a matter of discussion in the literature. Recent experimental evidence suggests that at low temperatures Ge(100) orders to a $c(4 \times 2)$ periodicity whereas at room temperature there is disorder and strong (2×1) features.[12-14] In Fig. 1 we present a series of He diffraction scans taken for different azimuthal angles and plotted versus the parallel momentum transfer $\Delta K_{\parallel} = (2\pi/\lambda)(\sin\theta_i - \sin\theta_r)$, where λ is the He wavelength, and θ_i and θ_r are the incident and reflected polar angles, respectively, measured from the surface normal. The scans are rotated in the plots to correspond to the appropriate azimuth, ϕ, thereby enabling a direct vertical correspondence with the reciprocal net as would be observed, for example, in normal incidence LEED, and which is schematically presented above the He diffraction scans. The schematic reciprocal net drawn is two-domain $c(4 \times 2)$ with the integer, half-order and quarter-order beams represented by squares of decreasing size. The experimental conditions for these He diffraction data are $\lambda \approx 1.0$ Å, $\theta_i = 60$°, and $T_s = 300$ K. The extra diffraction intensity not contained in the two-domain (2×1) net has been shaded in the figure for emphasis. This extra diffraction intensity is clearly observed as diffuse streaks extending from the half-order beam positions across the reciprocal net. Similar results have been obtained for several different Ge(100) crystals. These results are similar to but more detailed than those we observed for the Si(100) surface at room temperature.[4]

After several tens of Ar$^+$ sputtering and thermal annealing cycles, the streak intensity clearly increased, the extension in both dimensions became noticeably narrower, and the pattern became readily visible on the LEED display screen at room temperature. The LEED pattern showed the intensity of the streaks to be centered about the nominal quarter-order beam positions and did not completely extend to either the zone center or to the half-order beam positions. The streaks did not order into diffraction beams at room temperature. The He diffraction intensity at the center of the reciprocal net, however, is consistently higher than that in the nearby regions of the streaks. This suggests the presence of regions of another periodicity in addition to the disordered $c(4 \times 2)$, in particular to areas with a $c(2 \times 2)$ or $p(2 \times 2)$ structure. We observe this intensity at the net center for a number of incident angles and azimuths and particularly at low temperatures where the extent of the diffuse streaks is greatly diminished. We thus assign this extra intensity to small areas of an alternate structure which do not anneal away.

We have cooled the Ge(100) crystal to $T_s \approx 140$ K, maintaining the surface free of adsorbate contamination using yttrium aluminum garnet (YAG) laser irradiation

without significant laser-induced disorder, for times suffi-
ciently long to complete He diffraction scans.[14] In Fig. 2,
a series of scans obtained at $T_S = 300$ and 140 K are
directly compared. At low temperatures we observe the
streak intensity to sharpen into quarter-order beams corre-
sponding to the $c(4 \times 2)$ structure, but not to order com-
pletely. Compare the increase in the diffraction intensity
at the nominal quarter-order position with respect to the
half-order and integer peaks as the temperature is
lowered. Diffraction scans obtained for $T_S = 140$ K also
show the persistence of intensity at the zone center. This
can be seen for the scans A and D. In Fig. 3 we illustrate
various periodicities which may be related to these obser-
vations based on the tilted dimer model, and in particular
imply that a region of (2×2) periodicity is the origin of
the net center intensity.

The ordering of the $c(4 \times 2)$ lattice has been examined
as a function of crystal temperature. Results are shown in
Figs. 4 and 5. In Fig. 4 a series of polar-angle scans for
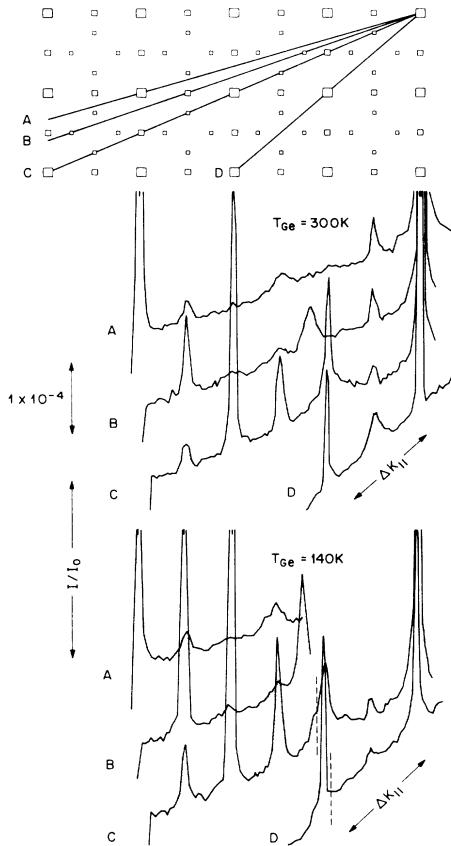$\theta_i = 26.6°$ are shown for a range of surface temperatures.

FIG. 2. Comparison of He diffraction scans obtained for a
Ge(100) surface at $T_S = 300$ K and $T_S = 140$ K for $\theta_i = 40°$,
$\lambda = 1$ Å. Pulsed laser irradiation enabled He diffraction mea-
surements to be made at surface temperatures < 300 K. The
portions of the spectra which appear to the right of the vertical
dashed lines in the lower set of spectra were taken while the
laser was blocked by the mass spectrometer detector and there-
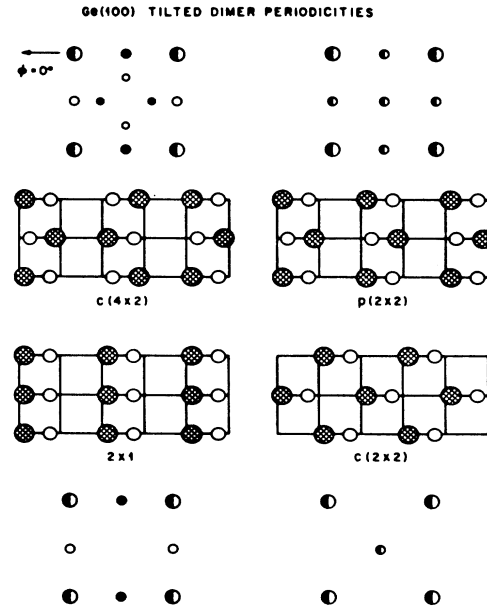fore the comparative intensities are only qualitative.

FIG. 3. Schematic geometry of the surface atomic layer and
associated reciprocal nets for various Ge(100) tilted dimer
periodicities. The large shaded circles represent atoms which
extend above the nominal unreconstructed surface plane. The
reciprocal nets correspond to the sum of two domains, each of
which is rotated by 90°. The contributions from each domain
are indicated by the white and dark regions, respectively. The
[$\bar{1}0$] crystallographic axis referred to in the text is along the
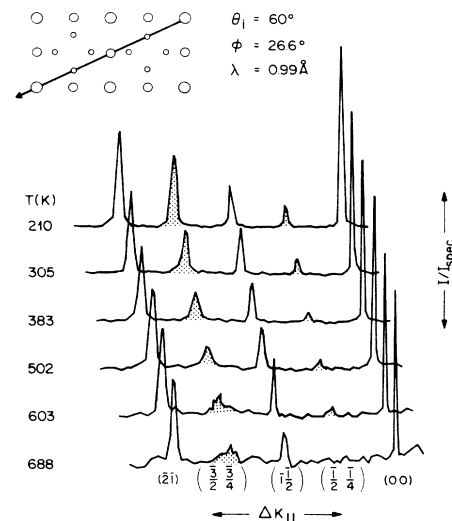direction of the $\phi = 0°$ azimuth.

FIG. 4. Temperature-dependent He diffraction of Ge(100)
for $\theta_i = 60°$ and $\phi_i = 26.6°$. The diffraction intensities have been
normalized to the specular intensity and are presented as a func-
tion of parallel momentum transfer. The direction of the scan
across the reciprocal net is shown in the inset. The quarter-
order peak intensities are seen to be much more temperature
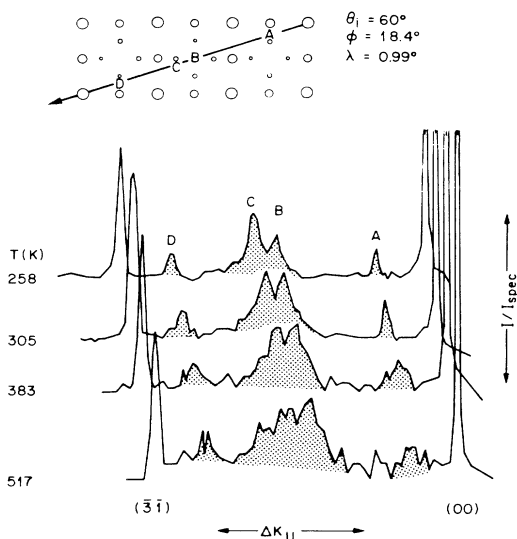dependent than are the half-order and integer features.

FIG. 5. Temperature-dependent He diffraction of Ge(100) for $\theta_i = 60°$, $\phi = 18.4°$. The scan transects several quarter-order streaks and also the center of the reciprocal net.

The intensities have been normalized to that of the specular beam, I_{00}, at the corresponding crystal temperature for the scan. This removes the dominant part of the Debye-Waller effect as is verified by the relative constancy of the integer beam intensities. The scans at $\phi = 26.6°$ cut through three integer beams and two quarter-order locations as previously shown in curve C of Fig. 1. The quarter-order intensity can be observed to be significantly diminished compared to the integer beams as the temperature increases continuously from 210 K, without an indication of a sharp transition temperature. Within our resolution there is no broadening of the quarter-order features. In contrast to this apparent continuous attenuation of quarter-order intensity we show the temperature dependence of the scattered intensity at the center of the net in Fig. 5. The He scattering intensity at the center of the net is substantial at $T_S = 140$ K (see Fig. 2, scan A) and does not attenuate significantly with increasing T_S as do the quarter-order features appearing in Fig. 4. Despite the increasing signal-to-noise ratio of the normalized higher temperature results, it is clear that the normalized intensity of the $(3\,\bar{1})$ peak is approximately constant and the intensity at the net center is not reduced. The trend in the streak intensity corresponding to positions A and D is not clear for the noise level shown. The results shown in Figs. 4 and 5 indicate that the complexities of the Ge(100) surface-ordering process are not likely to be well described by simple theories of order and/or disorder. It appears that there are patches of perhaps a (2×2) structure on the surface which do not easily anneal out at elevated temperatures. This suggests that lack of equilibrium due to high activation barriers may play a role in the ordering, particularly if $c(2 \times 2)$ regions are the source of the extra net center intensity rather than $p(2 \times 2)$. These presumed patches may be related to, or pinned to, a low density of defects or steps which may vary from crystal to crystal.

This is a similar conclusion to our previous hypothesis about disorder on the Si(100) surface.[4]

B. Diffraction scans

In Fig. 6, a sequence of diffraction spectra obtained for different incident polar angles along the $[\bar{1}0]$ azimuth $(\phi = 0°)$ at $\lambda = 0.99$ Å are presented. These spectra were obtained at room temperature, but the relative intensities do not change as the surface orders into a $c(4 \times 2)$ structure at lower temperatures. These spectra form the primary basis for the subsequent structural analysis. Several observations can be made upon inspection. For $\theta_i = 70°$ a maximum in the intensity envelope appears near $\theta_r = 0°$. This feature is a rainbow maximum which corresponds classically to scattering from the point of inflection in an oscillatory scattering potential. The slope of the potential at this point of inflection essentially determines the angular position of the diffraction rainbow maximum. Classically, the rainbow maximum moves with the incident beam angle so as to remain approximately at a constant angular separation from the specular beam in the absence of significant refraction from the attractive part of the potential. At $\theta_i = 60°$ a more complex rainbow maximum with an alternation in the adjacent beam intensities can be identified at $\theta_r \approx 0 - 10°$. At more normal angles of incidence the diffraction rainbow can no longer be observed due to an experimental cutoff. The appearance of a rainbow, far removed in angle from the specular beam, particularly at grazing incidence, is characteristic of an open and highly corrugated scattering potential surface with steep slopes.[17]

In Fig. 7 He diffraction scans obtained for a shorter wavelength beam, $\lambda = 0.57$ Å at $\theta_i = 70°$, $60°$, and $50°$ are
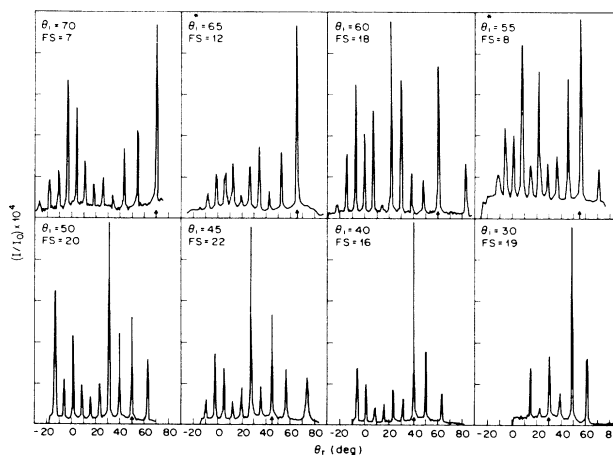

FIG. 6. He diffraction spectra taken in the $[\bar{1}0]$ direction $(\phi = 0.0°)$ for a series of incident angles θ_i. The upper angular limit is due to blocking of the incident beam by the mass spectrometer. The He wavelength was $\lambda = 0.99$ Å. The absolute full scale (FS) amplitude I / I_0 is indicated for each spectrum where I_0 is the intensity of the incident He beam. The data were obtained from two crystals, the first of which are marked by an asterisk $(\theta_i = 65°, 55°, \text{ and } 45°)$.
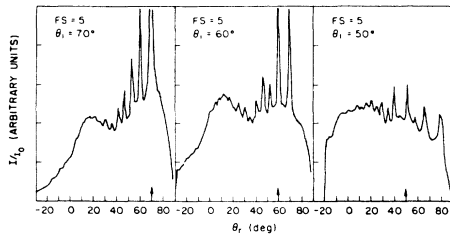
FIG. 7. He diffraction scans taken in the [$\bar{1}0$] direction for a series of incident beam angles θ_i, and an incident He wavelength of $\lambda = 0.57$ Å.

presented. At this shorter wavelength and correspondingly higher beam energy, the diffraction peaks are more closely spaced, the incident wavelength distribution is broader, and the ratio of inelastic to elastic scattering is greater. These conditions combine to yield a more continuous scattered distribution in contrast to the sharp diffraction beams of Fig. 6. However, the rainbow maxima are still identifiable and located in angle $\Delta\theta_{rb} \approx 50° - 60°$ from specular at $\theta_i = 60°$ and 70°, respectively. This small change in $\Delta\theta_{rb}$ from $\lambda \approx 1$ Å to $\lambda \approx 0.57$ Å confirms the rainbow assignment to these maxima. The small change in $\Delta\theta_{rb}$ may be associated in part with weakening of the refraction from the shallow attractive part of the He scattering potential (well depth $D \approx 5-10$ meV), and more subtly with the softness of the scattering potential and the increasing correspondence between classical and quantum scattering.

In Fig. 6 there is a sharp alternation in the rainbow region for $\theta_i = 60°$ for diffraction peaks between $\theta_r = 10°$ and $\theta_r = -20°$. This alternation in diffraction intensity is a characteristic of the rectangular two-domain surface. It indicates that the principle slopes in the scattering potential, and thus the rainbow angles for both domain directions, are comparable. Referring to Fig. 3 where the contributions to the diffraction intensities from each 90° domain orientation have been denoted by appropriate shading in the reciprocal lattice, note that both the (2×1) and $c(4 \times 2)$ periodicities have one domain contribute to all diffraction beams, whereas the 90° rotated domain contributes only to alternate or integer beams. This experimental alternation shows that the $p(2 \times 2)$ is not a substantial contributor to the diffraction spectra. In addition the alternation of beam intensity at the rainbow maxima provides a critical criterion for structural models as shown below.

From Figs. 6 and 7 a rough estimate of the degree of corrugation of the He scattering potential ξ can be obtained using a simple one-dimensional hard-wall sinusoidal corrugation function $f(x) = (\xi/2)\sin(2\pi x/L)$, where L is the repeat length. The value of ξ is obtained from $\Delta\theta_{rb}$ by considering local specular scattering for impact at the point of inflection with the result,

$$\xi = \frac{L}{\pi}\tan\left|\frac{\Delta\theta_{rb}}{2}\right| . \qquad (1)$$

If we assume the period L corresponds to the (2×1) re-

peat distance (see Fig. 3), then $L = 8$ Å for the [$\bar{1}0$] direction. For $\Delta\theta_{rb} \approx 50° - 70°$, $\xi_{(01)} = 1.2 - 1.8$ Å. For the $c(2 \times 4)$ periodicity ξ would be greater. Since the same slope occurs in the perpendicular direction, i.e., in the [01] direction for which $L = 4$ Å, we also estimate $\xi_{(01)} = 0.6 - 0.9$ Å. As we discuss below, although the scattering potential is not sinusoidal in shape, these estimates are qualitatively correct and correspond to a substantial opening of the surface potential topography compared to the unreconstructed surface. For comparison, the calculated peak-to-trough maximum corrugation of the unreconstructed Ge(100) surface is $\xi \approx 0.8$ Å.

In Fig. 6 secondary maxima can also be identified in the envelope of diffraction intensity, most dramatically for $\theta_i = 60°$ at $\theta_r \approx 20° - 30°$ and for $\theta_i = 50°$ and 45° at $\theta_r = 32°$ and 28°, respectively. These maxima may be attributed to supernumerary rainbow scattering which arises from interference *within* the unit cell due to impact parameters with equivalent classical scattering angles but with different classical path lengths. The extreme interference of this kind is for specular scattering from the flat top and bottom of an oscillatory surface potential, which yields the equivalent of Bragg's law $(2d\cos\theta = n\lambda)$ for constructive interference. Alternatively this second maximum may represent a second rainbow, i.e., a second point of inflection within the unit mesh. In either case it is indicative of a very corrugated open-surface potential. We are not able to definitively assign the physical origin of these secondary maxima although we are able to fit them.

IV. DISCUSSION OF EXPERIMENTAL RESULTS

These experimental results provide a number of conclusions about the Ge(100) surface without requiring diffraction calculations. The Ge(100) surface is disordered at room temperature, whereas below 150 K the surface is essentially ordered into a $c(4 \times 2)$. At 300 K the surface shows sharp (2×1) diffraction beams with additional narrow streaks of diffraction intensity extending through the quarter-order positions. The ordering improves continuously and not abruptly with cooling below room temperature. Intensity at the center of the reciprocal net persists at the lowest crystal temperature and also persists at high $(> 500$ K) temperatures indicating stable patches of another periodicity, possibly associated with or pinned to residual impurities, steps, or defects.

These results are essentially equivalent to, but more comprehensive than, our observations on the Si(100) surface. They indicate that the $c(4 \times 2)$ structure is a variation of the basic (2×1) structural unit. The surface is driven by a strong (2×1) primary reconstruction in the [$\bar{1}0$] direction with a weaker reconstruction in the [01] direction. The lack of registration of the weaker perturbation along the [01] rows leads to diffraction streaks. The narrowness of the streaks suggests a minimum length $(> 20$ Å) associated with the coherent domains of the secondary structure. These observations on the periodicity are well explained by the alternating tilted dimer model of the Ge(100) surface as sketched in Fig. 3 but are not unique to that model. The shape of the surface corruga-

tion as described below and confirmed by diffraction calculations, however, do indicate that the slightly tilted dimer is the basic unit in these structures. The identification of rainbows in the diffraction patterns obtained at grazing incidence show the He scattering potential to be highly corrugated and open in both the $[\bar{1}0]$ and $[01]$ directions. The depth of the corrugation in the $[\bar{1}0]$ direction is roughly 1.5—2.0 Å and perhaps half that in the $[01]$ direction based on the overlap of the $[\bar{1}0]$ and $[01]$ rainbows. The unreconstructed surface is estimated to have a maximum corrugation of ~ 0.8 Å. To obtain the large 2-Å corrugation, the surface must be opened substantially as in dimerization so as to expose deeper regions of the second layer. The results for both the periodicity and topography of Ge(100) are consistent with the alternating tilted dimer model. They suggest, as has been indicated theoretically for both of the Ge(100) and Si(100),[3,18−20] that the alternation of dimer tilting can create a range of periodic structures not very different in energy, which therefore can lead to a number of different ordered phases depending on small surface energy effects.

A. Theoretical comparison

In order to test structural models with He diffraction, a scattering potential must be generated. Theoretical considerations indicate that the repulsive part of the He-surface potential, which dominates the scattered angular distributions, is reasonably approximated as being proportional to the dilute-target charge density, i.e., $V(\bar{x}) = \alpha \rho(\bar{x})$, where $\alpha \approx 10^{5}$ meV/Å^{3}.[21,22] The most accurate available method for determining dilute surface charge densities ($\leq 10^{-5}$ a.u.) is the linear-augmented plane-wave (LAPW) technique.[23] However, the $c(4 \times 2)$ structure is too large for self-consistent LAPW calculations with available computational resources. We have previously shown that the simple approximation of spherical atomic charge superposition is substantially in error for reconstructed semiconductor surfaces.[1] We therefore make use of the modified atomic charge superposition (MACS) technique, developed for the Si(100) surface, in which effective surface atoms are defined for similar chemical environments. The charge densities of these atoms are calibrated with LAPW charge densities in a similar structural configuration for lower-order reconstructions of the Ge(100) surface. Specifically, we have calibrated effective Ge(100) surface atoms in a tilted dimer configuration for the (2×1) structure. We have previously shown for Si(100) that the parameters which describe the dilute charge region of these atoms are transferable to similar structures in other periodicities.

1. Modified atomic charge densities

A specific atomic configuration for the tilted dimer in which a dimer bond length of $d = 2.50$ Å and a tilt angle of $\theta_t = 12.2°$ was selected as a first basis for evaluation. The positions (x,y,z) of the four atoms which defined the dimer unit were set at $(0,0,0)$, $(0.45,0,1.40)$, $(2.86,0,0.87)$, and $(4.00,0,0)$ a.u. The atomic charge distribution parameters for the (2×1) Ge(100) surface were determined from a least-squares fit to LAPW charge contours. As was done for the analysis of Si(100) the Ge atoms were desig-

nated by their relative surface positions and were assumed to have a simple exponentially decaying charge distribution:

$$\rho_{at,i}(x,y,z) = \rho_{0i}\exp[-\kappa_i(r - r_0)] , \qquad (2)$$

$$r = [(x - x_a)^2 + (y - y_a)^2 + (z - z_a)^2(1 - \beta_i)^2]^{1/2} , \qquad (3)$$

where (x_a,y_a,z_a) are the nuclear positions for the type $i = $ I, II, and III atoms, which designate the upper and lower atoms of a buckled dimer, and all remaining bulk-like atoms, respectively. In addition to the decay constant, κ_i, and the prefactor, ρ_{0i}, a parameter describing the nonsphericity of the atomic charge distribution, β_i, is introduced. Depending upon the value of β_i, the charge density around each atom assumes a prolate or oblate aspect with respect to the surface-normal direction. The total charge density is then a sum of contributions from all atoms

$$\rho(r) = \sum_{i = I,II,III} \rho_{at,i}(r) . \qquad (4)$$

The resulting parameters which define the dilute charge region of the two surface atoms in the dimer, and the additional anisotropy required to fit the LAPW charge densities are given in Table I. As with Si(100), the relevant charge contours are relatively insensitive to the parameters of the second-layer atoms (atoms III). The fitting calculations used to optimize these parameter values were performed over a 20×10 mesh on the (2×1) surface cell for two LAPW surfaces of constant charge; $\rho = 1.0 \times 10^{-4}$ a.u. and $\rho = 3.0 \times 10^{-5}$ a.u. which approximately represent the classical turning point for scattering of He atoms in the energy range of interest. Examples of the charge-contour cross sections generated using the optimized parameters and the MACS procedure are presented in Fig. 8, where they are compared to contours generated by the LAPW method. The overall agreement is excellent. The optimized parameters are quite similar to those of Si(100) and reflect that the buckling of the dimer pair is associated with charge transfer to the uppermost dimer atom. The parameters reflecting the nonspherical extent of the atomic charge are consistent with the concept of the directional "dangling bond."

Using the optimized parameters presented in Table I, a MACS-surface charge contour for the $c(4 \times 2)$ periodicity

TABLE I. MACS parameters for the upper dimer (I), lower dimer (II), and bulk (III) Ge atoms.

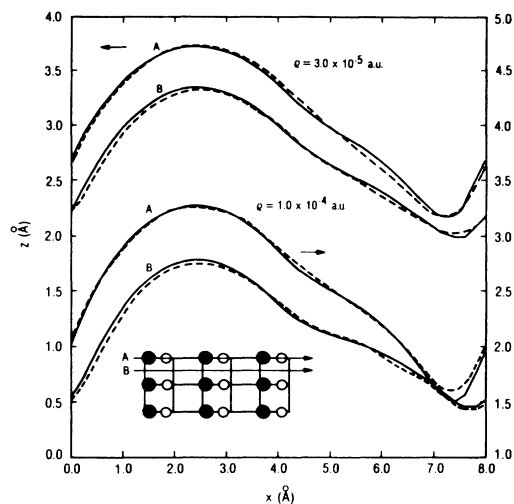| Parameters	Optimized value (a.u.)
κ_I	1.518
κ_{II}	1.507
κ_{III}	2.039
ρ_{0_I}	5.75×10^{-6}
$\rho_{0_{II}}$	5.07×10^{-6}
$\rho_{0_{III}}$	3.08×10^{-6}
β_I	7.91×10^{-2}
β_{II}	-1.41×10^{-2}
β_{III}	0 (fixed)
r_0	7.58

FIG. 8. Comparison of the charge contours of Ge(100) 2×1 obtained from LAPW (dashed line) and MACS (solid line) calculations at two charge densities. For each contour two cross sections are shown: (a) a cut through the (0$\bar{1}$1) plane containing dimer atoms, and (b) a cut through the (0$\bar{1}$1) plane passing through the second-layer atoms. Note that the contours at 1.0×10^{-4} a.u. refer to the scale on the right.

was generated. Eikonal scattering calculations[24] based on this model potential provided diffraction spectra for comparison with experiment. The charge contours used for the eikonal scattering calculations correspond to the classical turning point for the incident He atom assuming a hard wall potential $\rho = E/\alpha$, where the total He energy, E, is given by the incident beam energy E_i, and an assumed uniform attractive potential well depth D, such that $E = E_i + D$. D was set equal to 6.2 meV based on the laterally averaged potential calculated with the Laughlin formula[22] setting $C_6 = 21.6$ eV.

2. Surface topography

In order to have a visual reference for the sensitivity of He diffraction to different classes of model structures, in Fig. 9 we show calculated surfaces of constant charge density ($\xi = 4 \times 10^{-5}$ a.u.) for three examples: the unreconstructed surface, the (2×1) symmetric dimer, and the c(4×2) alternating tilted dimer surfaces. The peak-to-trough corrugation heights are also indicated for perspective. The surface dimerization of the (2×1) structure can be seen to open the surface thereby exposing deeper regions of the potential. The tilting of the dimer bond of 12°, and alternation of the tilt in the c(4×2), creates a larger open area increasing the total corrugation. The alternation of the dimer tilt has the effect of increasing the spacing of the atoms constituting the outermost atomic layer allowing greater penetration of the He atom. This larger and deeper open area is associated with an increased sensitivity to structure as discussed by Tersoff et al.[25] and directly shown below. Although the c(4×2) has a greater peak-to-trough corrugation amplitude, it is not clear that the slopes at the points of inflection are
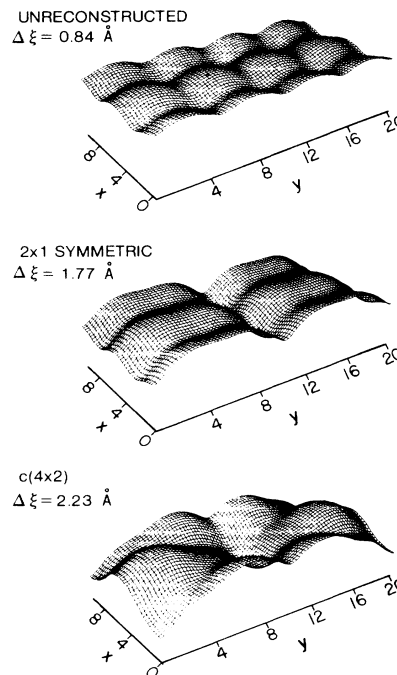

FIG. 9. Calculated charge density surfaces for the unreconstructed, symmetric (2×1) dimer reconstruction and asymmetric tilted dimer c(4×2) reconstruction of the Ge(100) surface at a charge density of $\rho = 4.3 \times 10^{-5}$ a.u. The scale perpendicular to the surface is amplified 4× with respect to that of the surface plane.

greater than those of the (2×1) symmetric dimer and thus rainbow maxima may occur at similar angles for each structure. However, the area around the point of inflection for the c(4×2) structure has considerably less curvature than that of the (2×1) and thus has much greater scattering power. This has important consequences in the comparison to experiment.

3. Diffraction calculations

We have calculated diffraction spectra for these structures using the eikonal scattering theory. The eikonal theory is a simple single scattering approximation which is quantitatively accurate only in the limit of weak corrugation.[24] However, the eikonal theory does yield essentially the correct positions for rainbow and supernumerary rainbows for highly corrugated surfaces, and we restrict ourselves to this type of comparison. Considering the approximations inherent in modeling the He-surface potential, particularly for complex structures, we think this is the optimum level of analysis.

In Fig. 10 we compare the qualitative features of the calculated diffraction patterns from the (2×1) symmetric, tilted, and c(4×2) tilted dimers with experiment for the incident angle range $\theta_i = 50°-70°$. The (2×1) symmetric dimer, like the unreconstructed surface (not shown), is relatively smooth, particularly in the integer direction, and has most of the scattering power near the
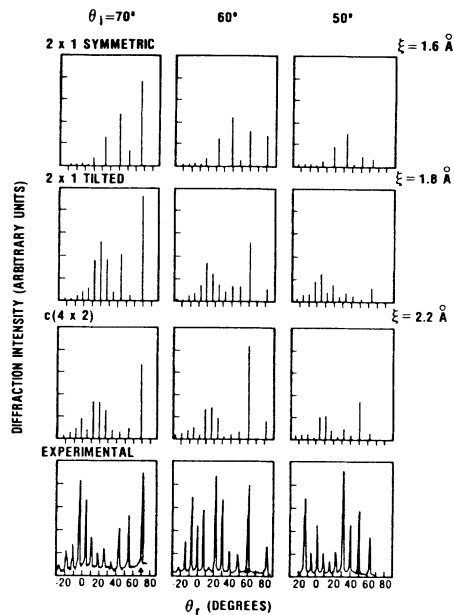
FIG. 10. Comparison of experimental and calculated diffraction spectra for various surface structures. The calculated diffraction spectra were obtained from domain averaged eikonal scattering from the respective MACS charge contours at $\rho = 4.3 \times 10^{-5}$ a.u. The maximum corrugation amplitude (peak-to-trough) ξ for the respective structures is also presented.

specular beam. Recall that the in-plane diffraction pattern from Ge(100) is a superposition of two directions (the [01] (half-order) direction and the [10] (integer) direction). The symmetric dimer scattering is dominated by the smooth [10] integer direction which has greater scattering power. In contrast the (2×1) tilted dimer has no mirror plane of symmetry so that the eikonal calculation averages all four [10] directions. At grazing incidence for the 2×1 tilted dimer there then appears a rainbow about 50° removed from the specular beam which corresponds to the more shallow-sloped point of inflection in the half-order direction. The steeper side of the dimer also generates a rainbow but it is located much farther from the specular beam ($\theta_r = -30°$ at $\theta_i = 70°$) and for which there is very little scattering power. Thus, the (2×1) tilted dimer diffraction pattern is dominated by the shallower side of the dimer and appears less corrugated than the data. The (2×1) tilted dimer does not generate the sharp alternation in the diffraction beam intensities best seen in the data at $\theta_i = 60°$. Along the dimer row the (2×1) tilted dimer is not sufficiently corrugated to generate a rainbow in the integer diffraction beams which overlaps with the rainbow of the more corrugated half-order direction. In contrast the $c(4 \times 2)$ does show this alternation indicating the alternation of the tilt provides the additional corrugation required for the integer direction. However, the agreement of this $c(4 \times 2)$ structure is only fair as the 12° tilt of the dimer bond results in too rough a scattering surface as we show below. In summary, only the $c(4 \times 2)$ alternating tilted dimer has sufficient corrugation in both directions

to have rainbows which come close to the experiment, but it does not fit the data particularly well for the dimer bond tilt angle of 12°. The $c(4 \times 2)$ structure preferred from this analysis is consistent with the observed ordering of the surface into a $c(4 \times 2)$ at low temperatures. We proceed with the $c(4 \times 2)$ tilted dimer structure and vary the model parameters.

4. Fit of the c(4×2) dimer structure

Simple considerations about He diffraction sensitivity to structure[25] suggest that the dimer tilt angle most strongly affects the degree of openness and thereby the slopes of the scattering potential. We have varied the tilt angle from 0°—12° and consider here only the results for $\theta_i = 60°$ where the experimental features are most clearly resolved. The dimer tilt was changed by a rocking motion in which the bond length, distance from the bond center to the third layer, and the positions of the third-layer atoms were fixed. As shown in Fig. 11, changing the tilt from 0°—10° yields a systematic trend in the angular positions of the rainbow maxima from each direction. As the tilt increases, the rainbow in the half-order direction eventually moves from the seventh to the eighth beam. The inner maximum moves from between the second and third beams from specular to merge with the outer rainbow maximum. At the same time the integer rainbow moves from the first beam to the second and third. All these changes are consistent with an increase in the openness and corrugation of the surface as the tilt increases. Considering only the angular positions of the maxima we conclude a tilt angle of 5°—7° is in acceptable agreement with the experimental data.

This result is supported by a comparison with the low-temperature diffraction data in the $[\bar{2}\bar{1}]$ direction, i.e., $\phi = 26.6°$, as shown in Fig. 4. Although this is a limited comparison, it should be sensitive to the degree of tilt as the alternating dimer tilt is directly responsible for the quarter order features of the data. As the surface nearly
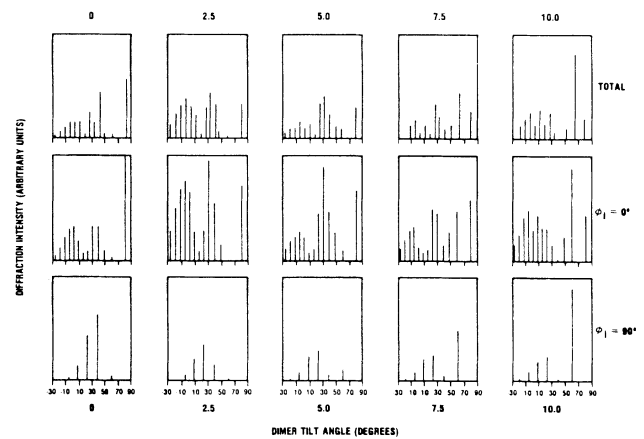

FIG. 11. Influence of the dimer tilt angle θ_t, on the calculated diffraction spectra in the $[\bar{1}0]$ direction. The spectra have been separated into the half-order and integer domain contributions. The conditions of the incident beam were $\theta_i = 60°$, $\lambda = 1$ Å.
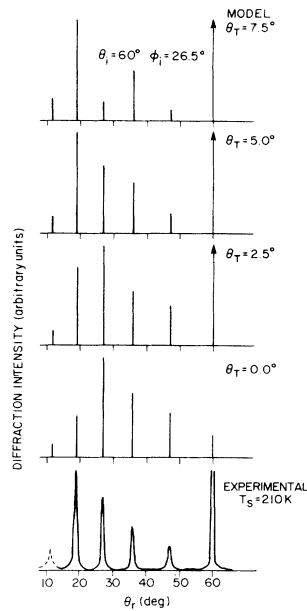
FIG. 12. Calculated diffraction intensities in the $[\bar{2}\,\bar{1}]$ direction for different values of the dimer tilt θ_t compared to experiment. The maximum value of the $(\frac{\bar{5}}{2}\frac{\bar{5}}{4})$ beam is estimated from Fig. 1 and dotted in.

orders the diffraction-beam envelope in the $\phi = 26.6°$ direction smoothly increases in intensity moving away from the specular beam. We can add additional information to Fig. 4 by considering Fig. 1 curve C, where we deduce that the intensity corresponding to the 5th diffraction beam, i.e., the $(\frac{\bar{5}}{2}\frac{\bar{5}}{4})$ beam, is much weaker than that of either the $(\frac{\bar{1}}{2}\frac{\bar{1}}{4})$ or the $(\frac{\bar{5}}{2}\frac{\bar{5}}{4})$ beams. Although the quarter-order features in Fig. 1 are not well ordered, the relative peak intensities of the diffuse beam intensities correspond well to the low temperature ordered surfaces. Consequently in Fig. 12 where we compare the results from the eikonal calculation for the $\phi = 26.6°$ direction with the data of Fig. 4 as a function of tilt angle θ_t, we also indicate and compare to the estimated maximum intensity of the $(\frac{\bar{5}}{2}\frac{\bar{5}}{4})$ beam. The calculations show a smooth and increasing envelope of diffraction beam intensities moving away from the specular beam with a maximum in the third beam for $\theta_t = 0°$. The maximum has moved to the fourth beam at $\theta_t = 5°$, whereas at $\theta_t = 7.5°$ the smooth structure collapses. A tilt of $\theta_t = 5°$ agrees well with the data in the $[\bar{2}\,\bar{1}]$ direction and is in good agreement with the range $\theta_t = 5°-7°$ inferred from the more detailed fit in the $[\bar{1}\,0]$ direction.

The calculated charge densities suggest a small charge transfer associated with the tilt of the Ge dimerized atoms in comparison to Si(100). We have examined the sensitivity of the fit to the extent of this transfer. Since the MACS atom parameters were calculated for $\theta_t = 12°$ and the optimum structure found is for $\theta_t = 6°$, the actual charge transfer should be less than that calculated. As a bound we have constrained the two dimer atoms to be equal in both size and decay rate to their calculated aver-

age values at $\theta_t = 12°$, and then recalculated the eikonal spectra corresponding to Fig. 12. We find for these equalized dimer atoms that the tilt must be increased to $\theta_t \geq 12°$ to achieve a sequence of diffracted intensities similar to that of the data. Thus an upper limit for the dimer tilt angle is $\theta_t \leq 12°$, and to the extent that MACS fit for 12° remains accurate small angles $\theta_t \rightarrow 6°$.

We have also looked at the effect of varying the dimer bond length on the calculated spectra over a range $2.15 < d$ (Å) < 2.85. Note the bulk Ge—Ge bond length is 2.45 Å. We find no substantial difference between the important features of the spectra for this range of bond length. We conclude that the He diffraction technique has insufficient sensitivity to meaningfully fit this parameter. We have also tested the sensitivity of the calculated spectra to the depth of the attractive well D. We have assumed throughout a simple uniform attractive well added to the hard wall repulsion for which the primary effect is refraction of the incident and exiting beams. Over a range $6 < D$ (meV) < 12 we find little effect on the positions of the rainbow maxima. In summary, a range of dimer bond lengths and attractive well depths have little influence on the fit to the primary features of the data or conversely He diffraction is insensitive to these parameters.

Calculated He diffraction spectra using a tilt of 6°, a bond length of 2.5 Å and $D = 6.6$ meV, are shown in Fig. 13 for $\theta_i = 70°-55°$, where they are directly compared to the corresponding experimental spectra. Excellent agreement is obtained at $\theta_i = 65°$, 60°, and 55°. At $\theta_i = 70°$ the agreement is not as good since the secondary maximum has not fully emerged from the specular beam in the data, but is well developed in the calculated spectra. This difference is likely a consequence of using a hardwall potential and not due to the geometry underlying the potential. A significant success of the model calculation is the ability to reproduce all of the qualitative features of the data including the intensity alternation for all θ_i.

V. CONCLUSION

The relative insensitivity of the He scattering potential to the details of the nuclear positions other than the tilt
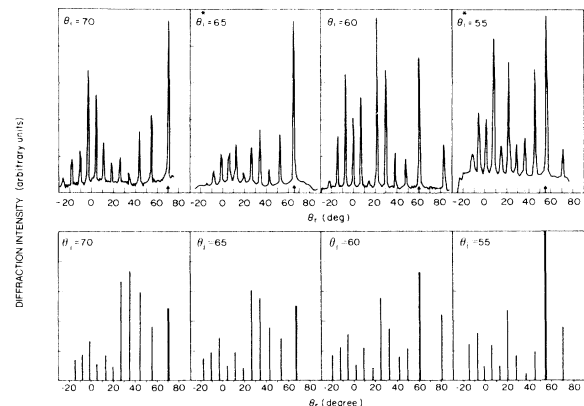

FIG. 13. Comparison of calculated and experimental diffraction spectra using structural parameters which provide the best fit for $\theta_i = 60°$.

angle demonstrates that the precise structure of any complicated surface cannot be determined based solely on He diffraction analysis. Only those factors which substantially influence the topography of the charge density surface at the $\rho = 10^{-5}$ a.u. level can be assessed. For the Ge(100) surface we find that the tilt of the dimer and consequent separation of the down atoms on adjacent dimers dominates the openness of the lattice. In addition, the effective slope of the surface, which is most important in obtaining correspondence between the calculated and experimental diffraction spectra, is sensitive to the height of the uppermost dimer atom which is affected by both the nonsphericity of the atomic charge and the charge transfer which is associated with the dimer tilt. A simple uncalibrated superposition of atomic charge densities would be totally inappropriate for this surface as illustrated by the sensitivity of the fit to the degree of charge transfer.

Despite what we think is a reasonably accurate determination of the repulsive part of the He-Ge(100) potential surface, errors inherent in the eikonal hard wall scattering theory, the inability to correctly treat the attractive part of the potential (including resonances), the effect of surface disorder, and the inexactness of the Debye-Waller approximation make further analysis of doubtful utility. However, the MACS scattering potential and the simple eikonal calculations do provide a reasonably accurate description of the experimentally observed primary and supernumerary rainbow positions in the [$\overline{1}0$] direction and the [$\overline{2}\,\overline{1}$] direction which are most related to the general topographical surface features. Hence, we conclude that the $c(4\times2)$ slightly tilted dimer model with a tilt angle of 6° is the best description of the Ge(100) surface based on He diffraction, and that He diffraction is sensitive to the details of the surface ordering and the tilt angle.

*On leave from the Institute for Solid State Physics, The University of Tokyo, 7-22-1 Roppongi, Minato-ku, Tokyo 106, Japan.

[1]A. Sakai, M. J. Cardillo, and D. R. Hamann, Phys. Rev. B 33, 5774 (1986).

[2]R. E. Schlier and H. E. Farnsworth, J. Chem. Phys. 30, 4 (1959).

[3]D. J. Chadi, Phys. Rev. Lett. 43, 43 (1979).

[4]M. J. Cardillo and G. E. Becker, Phys. Rev. B 21, 1497 (1980).

[5]J. J. Lander and J. Morrison, J. Chem. Phys. 37, 729 (1962).

[6]F. Jona, H. D. Shih, A. Ignatiev, D. W. Jepsen, and P. M. Marcus, J. Phys. C 10, L67 (1977).

[7]J. C. Fernandez, W. S. Ying, H. D. Shih, F. Jona, D. W. Jepsen, and P. M. Marcus, J. Phys. C 14, L55 (1981).

[8]F. Jona, H. D. Shih, D. W. Jepsen, and P. M. Marcus, J. Phys. C 12, L455 (1979).

[9]B. Z. Olshanetsky, S. M. Repinsky, and A. A. Shklyaev, Surf. Sci. 64, 224 (1977).

[10]T. D. Poppendieck, T. C. Ngoc, and M. B. Webb, Surf. Sci. 75, 287 (1978).

[11]M. J. Cardillo and W. R. Lambert, Surf. Sci. 168, 724 (1986).

[12]R. J. Culbertson, Y. Kuk, and L. Feldman, Surf. Sci. 167, 127 (1986).

[13]S. D. Kevan and N. S. Stoffel, Phys. Rev. Lett. 53, 702 (1984).

[14]W. R. Lambert, P. L. Trevor, M. T. Schulberg, M. J. Cardillo, and J. C. Tully, *Energy Solid-Beam Interactions and Transient Thermal Processing,* edited by D. K. Biégelsen et al. [Matr. Res. Symposia Proc. 35, 205 (1984)].

[15]R. M. Tromp, R. J. Hamers, and J. E. Demuth, Phys. Rev. Lett. 55, 1303 (1985).

[16]M. J. Cardillo, C. S. Y. Ching, E. F. Greene, and G. E. Becker, J. Vac. Sci. Technol. 15, 423 (1978).

[17]M. J. Cardillo, S. J. Sibener, G. E. Becker, and D. R. Miller, Surf. Sci. 107, 469 (1981).

[18]J. Ihm, D. H. Lee, J. D. Joannopoulos, and A. N. Berker, J. Vac. Sci. Technol. 31, 705 (1983).

[19]J. Ihm, D. H. Lee, J. D. Joannopoulos, and J. J. Xiong, Phys. Rev. Lett. 51, 1872 (1983).

[20]M. T. Yin and M. L. Cohen, Phys. Rev. B 24, 2303 (1981).

[21]N. Esbjerg and J. K. Norskov, Phys. Rev. Lett. 45, 807 (1980).

[22]R. B. Lauglin, Phys. Rev. B 25, 2222 (1982).

[23]D. R. Hamann, Phys. Rev. Lett. 46, 1227 (1982).

[24]U. Garibaldi, A. C. Levi, R. S. Spadicini, and G. E. Tommei, Surf. Sci. 48, 649 (1975).

[25]J. Tersoff, M. J. Cardillo, and D. R. Hamann, Phys. Rev. B 32, 5044 (1985).